In-situ SAXS/WAXS investigations of the mechanically-induced phase transitions in semi-crystalline polyamides

Julie Pepin, Valérie Gaucher, Cyrille Rochas, Jean Marc Lefebvre

In-situ SAXS/WAXS investigations of the mechanically-induced phase transitions in semi-crystalline polyamides

Julie Pepin[1], Valérie Gaucher[1*], Cyrille Rochas[2] and Jean-Marc Lefebvre[1]

[1] *Univ. Lille, CNRS, INRA, ENSCL, UMR 8207 - UMET - Unité Matériaux et Transformations, F-59000 Lille, France*
[2] *CERMAV, UPR 5301 CNRS, Grenoble, France*

*: Corresponding author

Valerie Gaucher

Univ. Lille, CNRS, INRA, ENSCL, UMR 8207 –
UMET - Unité Matériaux et Transformations, F-59000 Lille, France
Tel: +33-320-336416

e.mail: valerie.gaucher@univ-lille.fr

ABSTRACT: The structural evolution under uniaxial tension of both Polyamide-11 (PA11) and Polyamide-6 (PA6) crystallized under various crystal forms has been investigated as a function of draw temperature with respect to the Brill transition. The use of in-situ synchrotron two-dimensional wide-angle X-ray diffraction and small-angle X-ray scattering allows to discriminate thermal from mechanical effects, leading to a revisited scheme of the strain-induced phase transitions in polyamides. It is demonstrated that only the H-bonded sheet-like structures transform mechanically into a pseudo-hexagonal form with a random distribution of H bonds around the chain axis. This order-disorder transition occurs during the fibrillar transformation and seems systematically preceded by a twinning mechanism at low deformation. By contrast, the mesophases and the High Temperature forms are mechanically stable, the latter transforming thermally into the H-bonded sheet-like structures as soon as samples are cooled down below the Brill transition temperature.

Introduction

Aliphatic polyamides are widely used in various fields such as food packaging, automotive or textile for their relatively good mechanical properties. Nonetheless, these mechanical properties are strongly sensitive to the environmental conditions [1,2] and to the initial crystalline structure as well [3-5]. Indeed, aliphatic polyamides display at room temperature an important polymorphism arising from the optimization between chain conformation and hydrogen bond energies, depending on the crystallization conditions [6-9]. Even if crystalline structures are different for each aliphatic polyamides, one may notice some common features among them. The α phases are characterized by chains in all trans planar conformation with an organization of the H-bonds within sheets held together by van der Waals interactions. Depending on the crystallization conditions, various α phases characterized by different degrees of perfection may be obtained at room temperature. Thus, in the case of polyamide 11 (PA11), a "perfect" α phase is obtained by solution casting using m-cresol [10,11] whereas a less perfect structure called α' arises from slow cooling from the melt [10, 12-14]. Similarly, in polyamide 6 (PA6), it is possible to achieve different α phases with varying crystal perfection, depending on the crystallization protocol. Moreover, both PA11 and PA6 display another sheet-like structure with a chain twist in the amide groups with respect to the methylene segment [15-18] but these γ phases will not be investigated in the present work. In addition to these ordered structures, aliphatic polyamides may crystallize into mesophases, PA11-δ' [19-20] and PA6-β [21-22], characterized by a pseudohexagonal unit cell with a random distribution of the H-bonds around the chain axis [23-25]. These mesophases are obtained after quenching from the melt [16,26-27]. Table 1 summarizes the unit cell parameters of these various polymorphs according to literature.

Table 1. Unit cell parameters of PA6-α, PA6-β, PA11-α and PA11-δ'.

Crystalline structures		Unit cell parameters						References
		a (Å)	b (Å)	c (Å)	α ()°	β (°)	γ (°)	
PA6-$\alpha^{(a)}$	Monoclinic	9.56	17.2	8.01	90	67.5	90	21
PA6-$\beta^{(a)}$	Pseudohexagonal	9.6	17.2	9.6	90	60	90	23
PA11-$\alpha^{(b)}$	Triclinic	9.8	5.25	14.9	50.5	90	72	28
PA11-$\delta'^{(b)}$	Pseudohexagonal	4.22	4.22	12.9				19

(a): in PA6, the chain axis is along the b direction (b): in PA11, the chain axis is along the c direction

Some polyamides are also known to display a thermally-induced phase transition, called the Brill transition [29-31]. This transition is well documented in the case of PA11 [10,32], while its existence

has been a matter of debate in PA6 for several decades [33-35]. Evidences for its occurrence has been provided more recently [36]. When a sheet-like structure is heated above the Brill transition temperature, it transforms into a pseudohexagonal high temperature (HT) structure (PA11-δ or PA6-β') in which the H-bonds are randomly distributed around the chain axis. Upon cooling this transformation is reversible. In a recent contribution, we have demonstrated that the occurrence of the Brill transition strongly depends on crystal perfection of the H-bonded sheet-like structure: the Brill transition temperature increases with perfection of the α phase in such a way that the perfect phase keeps its lattice symmetry up to the melting point. Regarding the mesophases, they also transform into the HT structures. These thermal transitions have a more or less marked signature in thermal analysis. In particular, the transformation PA6-β $\rightarrow$ PA6-β' is characterized by a broad exotherm between 100 and 190°C, indicative of a progressive evolution of the crystal structure as the temperature is increased.

Polymorphism and thermally-induced phase transitions strongly impact the mechanical properties of aliphatic polyamides. In particular, previous work has underlined that samples displaying H-bonded sheet-like structure cannot be biaxially stretched, contrary to the mesostructures [37]. Furthermore, it has been shown that plastic deformation of polyamides may be accompanied by mechanically-induced phase transitions. Numerous post-mortem studies report some order-disorder, disorder-order and order-order crystal phase transitions, depending on the initial crystalline structure and stretching conditions [38-45]. For example, Zhang et al have shown in PA11 an order-disorder transition during uniaxial drawing at low temperature whereas the mesophase remains mechanically stable [40]. In the case of PA6, a γ->α transition has been reported upon drawing below the glass transition temperature as well as at high temperature [5,41-42]. Moreover, others studies devoted to PA6 have revealed a mechanically-induced β->α transition whatever the drawing temperature [43] while another investigation on PA6-α has shown an order-disorder transition during uniaxial stretching [44]. In the case of PA6-γ fibers uniaxially drawn, Murthy also observed a transformation from γ phase into a metastable structure [45]. This brief overview based on the post-mortem studies is quite puzzling: it seems that deformation induces some order-disorder transitions as well as disorder-order ones. While the interpretation of the diffractograms recorded at room temperature for samples stretched below the Brill transition is quite clear, those relative to HT stretching are complex due to the superposition of both thermal and mechanical effects. Therefore, the use of in-situ measurements is required to clearly identify the strain-induced structural evolution in aliphatic polyamides. This experimental approach has become very common in recent years [46-49]. For example, in-situ analyses were performed by Xu on stretched PA6 samples but only focusing on the crystal structure evolution upon heating of these oriented materials; the stretching step was not in-

situ monitored by SAXS/WAXS experiments [46]. Another recent contribution was devoted to the tensile deformation of polyamide 6 studied by both in-situ SAXS and WAXS measurements but focused on the preyield strain range [49].

In this context, use of in-situ SAXS/WAXS structural characterization is aimed at revisiting the mechanically-induced phase transitions as a function of temperature in both PA11 and PA6. The present work focuses on the uniaxial tensile behavior on both sides of the Brill transition temperature with special attention paid to the role of the initial crystal structure.

Experimental section

Materials and preparation

The polyamide 11 (PA11) under investigation is a commercial grade material from *Arkema* (Serquigny, France) having a weight-average molar weight $M_w \approx 25\ 000$ g.mol^{-1}. The α crystals were obtained by casting from a 5wt % solution in m-cresol at around 150°C and then by drying for two weeks at 80°C under primary vacuum to remove moisture and solvent traces. Films with a thickness of 100 μm crystallized under α' and δ' phases were prepared by compression-molding at varying cooling rate. PA11-α' and PA11-δ' were obtained by cooling down to room temperature (RT) at 2°C.min^{-1} and by quenching in an ice bath, respectively.

The polyamide 6 (PA6) used in this study under trade name *Akulon F130* from *DSM* (Geleen, the Netherlands), has a number-average molecular weight $M_n = 25\ 600$ g.mol^{-1}. Samples were supplied by DSM in the form of 130 μm thick films in an amorphous state. This film was obtained by extrusion at 270°C on a chill roll at 20°C and was then annealed using different procedures to obtain various crystal polymorphs. Thereby, samples in predominantly mesomorphous β form (PA6-β) have arised from an annealing of the initial cast film at 80°C for 10 min whereas films in predominantly α phase have been obtained by annealing at 190°C for 10 min.

Polyamides are known to be strongly sensitive to moisture due to their H-bonds. Since the water content has a great influence on the mechanical properties [1-2], it was chosen to keep all samples under vacuum at room temperature (RT) prior to any test in order to characterize them in a dry state.

Differential Scanning Calorimetry (DSC)

Thermal analysis was performed on a DSC7 apparatus from PerkinElmer calibrated with indium. The 10 mg samples were scanned at a heating rate of 10°C.min^{-1} under nitrogen gas flow. The crystalline weight fraction was computed from the enthalpy of the melting endotherm using the melting enthalpy of 100% crystallized PA11 $\Delta H_m^0(PA11)$ =226 J.g^{-1} [50] and $\Delta H_m^0(PA6)$ = 230 J.g^{-1} [51] whatever the crystalline form.

Mechanical behavior

Uniaxial drawing experiments have been carried out on a Instron 4466 tensile testing machine equipped with a temperature controlled chamber regulated at ±1°C. All samples were drawn in the dry state in a temperature range between 80°C and 165°C for PA11 and 55°C and 190°C for PA6. Tensile specimens with 22 mm gauge length and 5 mm width have been stretched with an initial deformation speed of 10^{-2} s^{-1}. For each condition at least 3 samples were tested to ensure reproducibility.

Structural characterization

The structural evolution upon stretching was followed in-situ by means of Wide-Angle X-ray scattering (WAXS) and Small-angle X-ray scattering (SAXS) using synchrotron radiation on the BM02 beamline at European Synchrotron Radiation Facility (Grenoble, France). A homemade stretching device with symmetrical drawing adaptable on the synchrotron beamline and equipped with a hot-stage thermal control unit able to heat up to 145°C was used. The symmetrical drawing allowed to keep the same region of the sample in front of the X-ray beam. For these experiments, dumbbell shaped samples with dimensions of 12 x 4 mm² were stretched with an initial deformation speed $\dot{\varepsilon}_0$ of 10^{-2} s^{-1} (identical to ex-situ uniaxial tests) at temperatures on both sides of the Brill transition for PA11 and PA6.

WAXS experiments were performed using an energy of 22 keV (i.e. λ= 0.56 Å) while an energy of 8 keV was used for the SAXS analysis (i.e. λ = 1.54 Å). Through-view 2D-patterns were recorded using a CCD camera from Princeton Instruments. Standard corrections were applied to the patterns before their treatment.

In the case of WAXS experiments, the sample-detector distance was calibrated using a PLA sample. The scattering vector range was 0.10 <q (Å^{-1}) < 2.25. In the paper, all WAXS diffractograms are expressed in terms of 'equivalent scattering angle 2θ' corresponding to radiation wavelength λ = 1.54 Å. The WAXS exposure time was 5 s with a delay time of 5 s necessary for downloading the pattern. The intensity profiles were obtained by azimuthal integration of the 2D patterns using the

fit2D software. The intensity profiles have been classically computed from the overall integration of the image from φ=0 to φ=360° (referred to as 360°-integration).

The resulting intensity profiles were treated using Peakfit software: in the case of PA11, Pearson VII functions were chosen to fit the amorphous halo and Gaussian profiles were used for scattering peaks whereas for PA6, Pearson VII functions were selected for both amorphous halo and diffraction peaks.

As in previous work [36], the crystalline perfection of the H-bonded sheet like structures has been estimated from the gap between the two main diffraction peaks. The crystal perfection index (CPI) is defined as:

$$CPI = \frac{\left(\dfrac{d_{200}}{d_{210/010}}\right) - 1}{\Omega}$$

where d_{200} and $d_{210/010}$ are the interplanar spacings for (200) and (210)/(010) planes respectively. Ω is a constant equal to 0.189 for PA11 and 0.194 for PA6 so that CPI = 1 in the case of the so-called "perfect" α phase for each material. That is to say, the α structure obtained by solvent-casting in m-cresol for PA11 [36] and the one described by Holmes et al in the case of PA6 [19].

In the case of SAXS experiments, the q scale was calibrated using a silver behenate reference sample and the scattering vector q range was $0.02 < q$ (Å^{-1}) < 0.12. Concerning semi-crystalline polymers studied by SAXS, scattering arises from the periodic stacking of alternating amorphous and crystalline regions thanks to the electron density contrast between these two phases. This leads to a correlation peak observed perpendicularly to the lamellae surfaces [52] from which we can deduce the so-called long period L_p and the orientation of the lamella:

$$L_p = \frac{2\pi}{q_{max}}$$

where q_{max} is the value of the scattering vector at the maximum of the Lorentz plot $I(q) \times q^2 = f(q)$ of the intensity profile.

Results and discussion

Structural characterization of PA11 and PA6

Figure 1 displays the integrated intensity profiles from WAXS patterns for the undeformed films of both PA11 and PA6. The mesomorphous structures are characterized by a broad reflection located around $2\theta \approx 21.5°$ whereas the sheet-like structures diffraction profiles display two well defined

peaks located at $2\theta \approx 20°$ and $23.5°$ for PA11 and $2\theta \approx 20°$ and $24°$ for PA6 respectively. It is worth reminding that the reflections at $2\theta \approx 23.5°$ and $24°$ for PA11 and PA6 respectively refer to the H-bonded planes. It is worth recalling that we consider the perfect α phase for PA6 as the one described by Bunn [21] and in the case of PA11 the phase obtained by solvent casting from m-cresol [36].
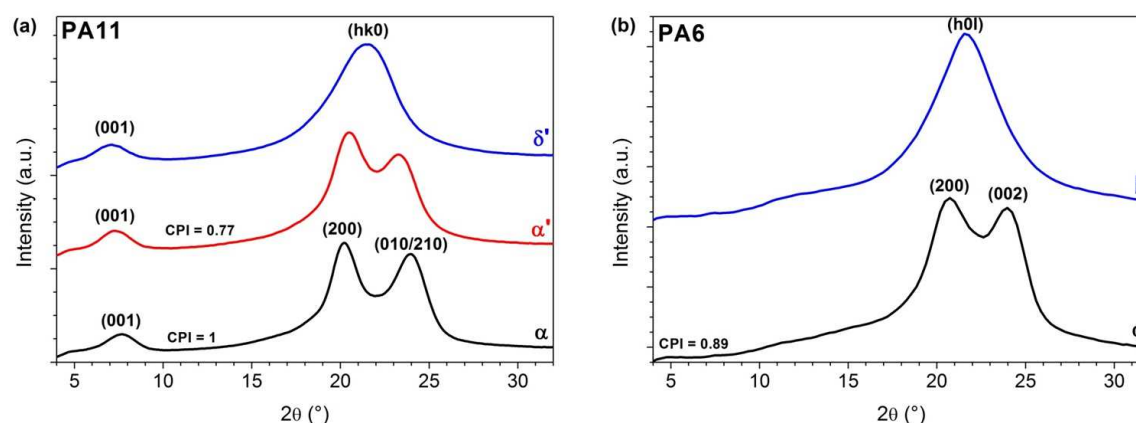

Figure 1. Diffractograms recorded at room temperature of (a) PA11 and (b) PA6 crystallized under various crystalline forms.

Otherwise, SAXS experiments have revealed an isotropic distribution of regularly stacked lamellae. Long periods as well as thermal characterizations of samples are reported in Table 2. All samples exhibit similar glass transition temperature and crystallinity except for PA11-α which displays a higher crystal index related to its elaboration mode.

Table 2. Thermal and structural characterizations for both PA6 and PA11 samples (Accuracy ± 1 °C for temperature and ± 2% for crystal content – see Supporting Information).

		T_g (°C)	χ_c (%)	CPI	L_p (nm)
PA6-α	H-bonded sheet-like structure	50	35	0.89	8.1
PA6-β	Mesophase	51	29	/	5.2
PA11-α	H-bonded sheet-like structure	53	41	1	10.5
PA11-α'	H-bonded sheet-like structure	52	29	0.77	9.6
PA11-δ'	Mesophase	52	25	/	8.5

The thermal stability of all these structures has been reported in a previous paper [36]. To summarize, both mesophases (PA11-δ' and PA6-β) display a Brill transition whose temperature onset

is around 100°C. The mesophases evolve towards a HT structure named PA11-δ and PA6-β'. It is worth reminding that in the case of PA6-β, this transition occurs gradually in the broad temperature range between 100 and 190°C. When cooled down to room temperature, the HT structures transform into a H-bonded sheet-like structure, the CPI of the final structure depending on the maximum temperature reached during heating. Regarding the H-bonded sheet-like structures, it was highlighted that the perfect α phase is thermally stable up to the melting point (PA11-α). By contrast, the less perfect sheet-like structures turn into the same HT phase as in the case of mesophases and the transition temperature depends on the CPI of the initial phase. Thus, it was identified around 165°C for PA6-α and 100°C for PA11-α'.

Mechanical behavior

Figure 2 depicts the uniaxial tensile behavior of both PA11 and PA6 as a function of temperature for samples crystallized under different polymorphs. For both materials, the temperature range under concern spans from the glass transition temperature up to the melting point. Except in the case of PA6 drawn at 55°C (i.e. just above T_g), it may be considered in a first approximation that the amorphous phase is in a true rubbery state and therefore does not control plastic yielding.

Apart from PA11-α stretched at 80°C, all samples exhibit a ductile behavior, whatever the initial crystalline form. In particular, the less perfect H-bonded sheet-like structure, PA11-α', drawn below the Brill transition displays a strain at break value exceeding 300%. Although the H-bonded sheet-like structures are unable to sustain biaxial stretching [37,53], these results indicate that they may be uniaxially drawn. One may notice that for both polyamides, the sheet-like crystalline structures PA11-α' and PA6-α exhibit a larger yield stress and a lower strain at break than in the case of theirs mesomorphic structures. The lower ductility of the H-bonded sheet-like structures, as compared to the mesophases has already been reported in PA6 [5]. As the temperature is increased, the stress-strain curves gradually merge into a unique mechanical response for each polyamide, irrespective of the initial crystalline form. This is the sign of the thermal transformation of the less perfect sheet-like and mesomorphic structures into the high temperature form [36]. It is worth noting that in the present case the thermal transformation of the less perfect structures into the HT structure is not accompanied by an abrupt improvement in drawability, as observed for the biaxial stretching behavior [37].
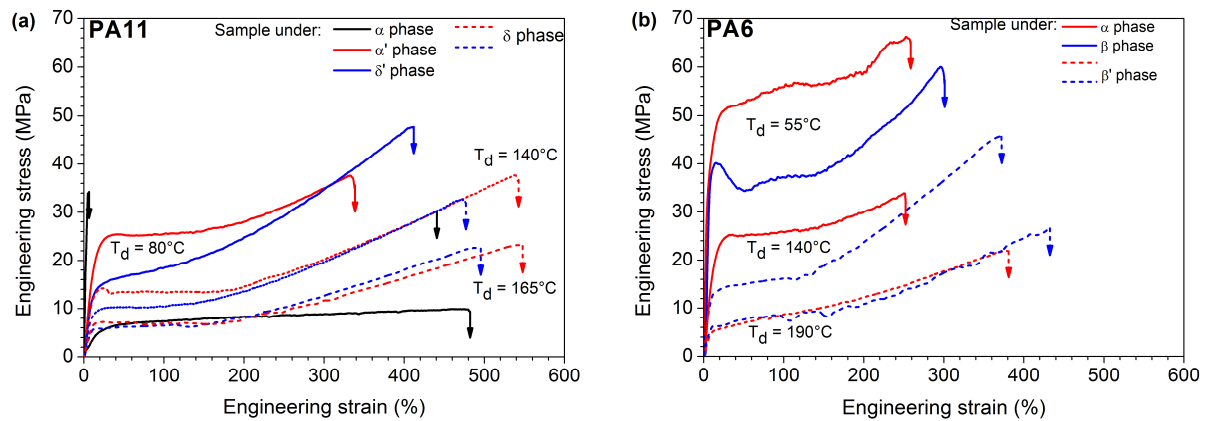
Figure 2. Mechanical behavior under uniaxial drawing of (a) PA11 and (b) PA6 samples as a function of both initial crystalline structure and temperature

Most curves display a significant strain-hardening related to macromolecular network orientation during the fibrillar transformation as clearly assessed in literature for polyamides (see e.g. [54,55]). In the following, focus is put on the understanding of crystal phase evolution upon drawing below and above the Brill transition. For this purpose, in-situ SAXS/WAXS experiments have been performed on both PA6 and PA11 polymorphs with the aim of outlining general trends of behavior.

Structural evolution

Considering the ratio between width (w) and thickness (t) of the sample (w/t ≈ 40), through and edge view 2D patterns were recorded with the X-ray beam normal and parallel to the film surface respectively. The similar patterns confirm cylindrical symmetry around the draw axis of the sample. Accordingly, in the following, only the through views are presented.

Strain-induced phase transitions below the Brill transition

Figure 3 reports the WAXS patterns recorded at various draw ratios together with the integrated intensity profiles for PA11-δ' stretched at 80°C. As expected, upon drawing, chains are gradually aligned in the draw direction, as indicated by both the orientation of the (001) reflection in the polar direction and the strong equatorial reinforcement of the diffraction peak (hk0) (chain axis lies along the c direction) (Figure 3.a). As the draw ratio is increased, the 360° integrated profiles (Figure 3.b) show a gradual shift of the (001) reflection towards lower Bragg angles in relation to the extension of the chains in the tensile direction. Additionally, the progressive broadening of the main scattering in the equatorial position reveals a loss of order in the (hk0) planes assigned to a decrease of the coherent domain sizes. The quantitative analysis based on the deconvolution of the integrated intensity profiles (Figure 3.c), shows that deformation of PA11-δ' induces a decrease from 5 to 3 nm

of the coherent domains size in [hk0] directions and a crystallinity increase up to 10% at the end of drawing. The latter result was also confirmed by thermal analysis. Therefore, no evidence of strain-induced crystal phase transition is provided by WAXS analysis for the smectic form of PA11.
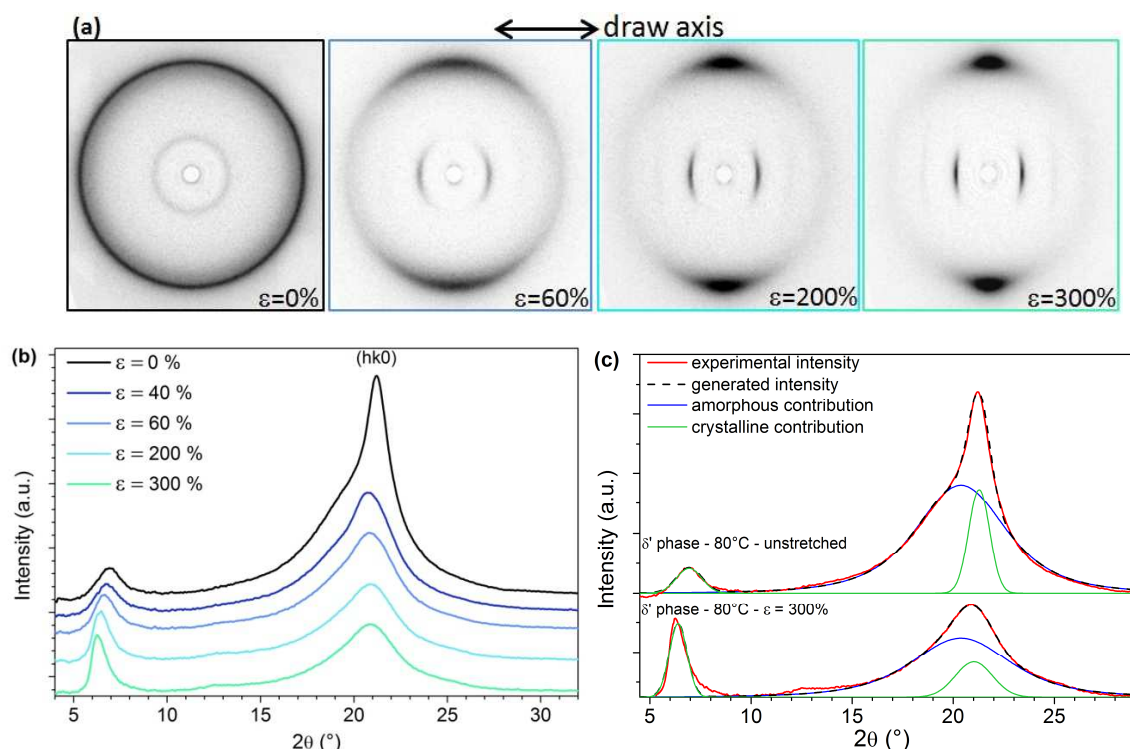

Figure 3. (a) In-situ WAXS patterns of PA11-δ' stretched at 80°C as a function of the engineering strain, (b) evolution of diffractograms and (c) curve-fitting analysis of both unstretched and stretched samples

The SAXS patterns are reported in Figure 4 as a function of strain in the case of PA11-δ'. Initially (ε = 0%), the pattern shows an isotropic distribution of the crystallites which are regularly stacked with L_p = 8.5 nm as previously mentioned in Table 1. For ε = 45%, the initial circular ring transforms into an ellipse reflecting an increase in the long spacing in the polar direction and the reverse behavior in the parallel direction. This phenomenon has already been reported in literature for several semi-crystalline polymers such as polyethylene [56] and PA6 [49]. During stretching, stacks of lamellae are not submitted to the same loading according to their orientation with respect to the draw axis. In the case of a spherulitic structure, the lamella stacks in the equatorial regions of the spherulite are subjected to tensile stress while those in the polar regions undergo compression due to the Poisson effect. As the draw ratio is increased, crystalline lamellae tend to orient perpendicular to the stretching direction as indicated by the polar scattering (Figure 4.c). As high draw ratio (ε =300%), scattering gets weaker probably due to the decrease in sample thickness but this phenomenon may also suggest a loss of the regular crystal/amorphous stacks with drawing.
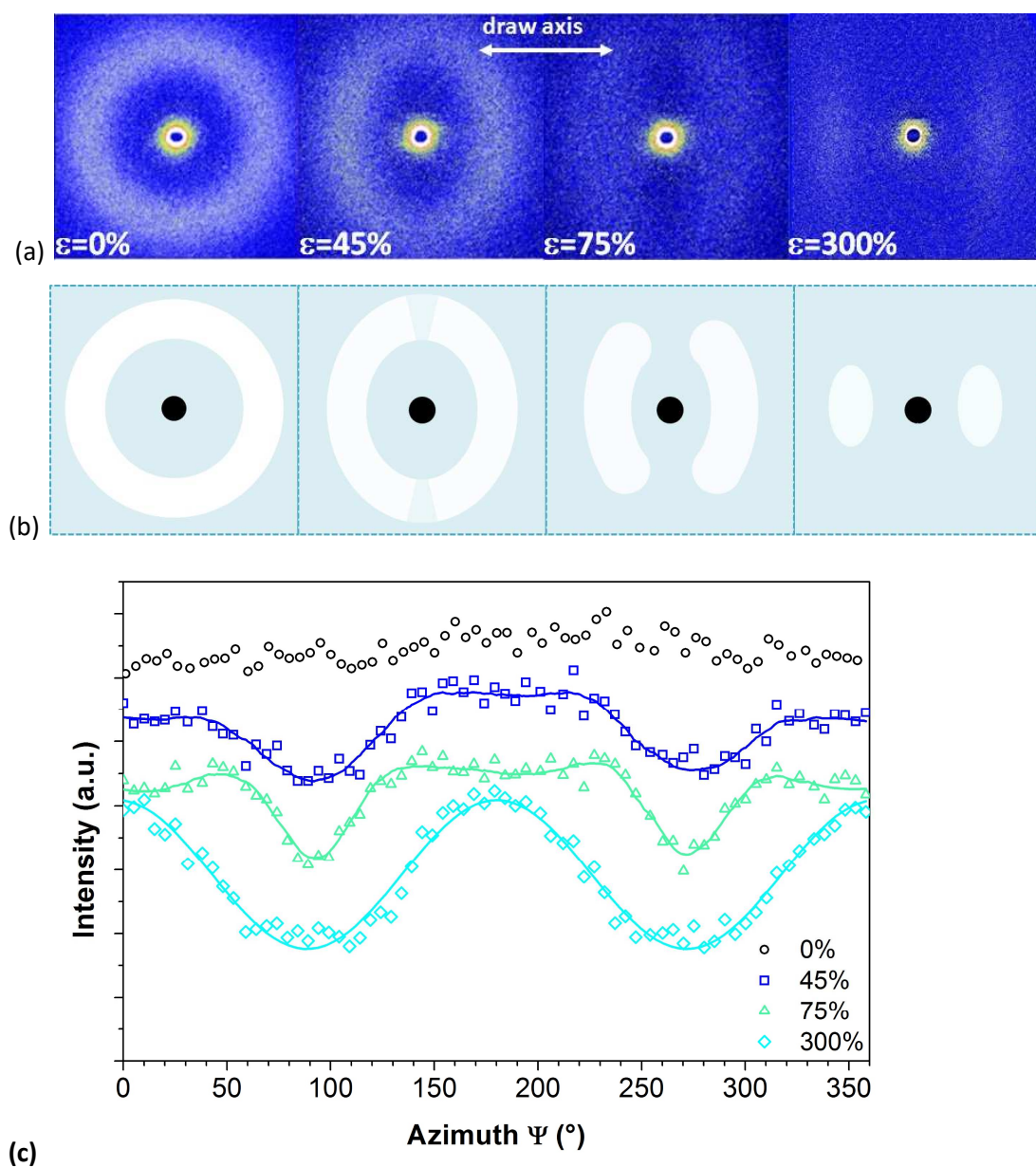
Figure 4. (a) In-situ *SAXS patterns (b) scheme of SAXS patterns and (c) scattering intensity as a function of azimuthal angle Ψ of PA11-δ' uniaxially stretched at 80°C. (Ψ = 0/180/360° correspond to the draw axis)*

In summary, the SAXS/WAXS analysis of PA11-δ' upon drawing does not reveal any mechanically-induced phase transition, i.e. it assesses that the smectic phase of PA11 is mechanically stable.

Similar results are observed for PA6-β stretched at 80°C: no phase transition is evidenced from SAXS/WAXS pattern analysis (see Supporting Information) therefore establishing that the PA6 mesophase is mechanically stable as well.

Figure 5-a depicts the evolution of the diffraction patterns of PA11-α' as a function of draw ratio. In addition to a gradual orientation of the macromolecular chains towards the draw axis, the two reflections characteristic of the α' phase gradually disappear, resulting in a unique broader

diffraction. Moreover, based on the deconvolution of diffractograms (not shown here), it appears that crystallinity remains constant around 30%. These results indicate that there is no destruction of crystals upon stretching but that we are dealing with an order-disorder transition. This phenomenon, may be attributed to an accumulation of plasticity defects in the crystals, as already reported for EVOH [57] and PA6-α [58], leading to the formation of a mesophase which looks like the smectic δ' form. Indeed, comparison of the diffractograms of PA11-δ' and PA11-α' stretched up to 200% shows that the crystalline structures of both samples are similar (Figure 5-b). This confirms that a PA11-α'→PA11-δ' transformation has occurred upon drawing. Note that similar observations have already been reported for PA12-12 from in-situ WAXS experiments: the triclinic α-form is mechanically transformed into a mesomorphic phase under uniaxial tension [48].

In order to get further information about the origin of the strain-induced crystal change, specific attention has been paid to the patterns recorded at low strains. During the first stage of deformation (ε=20%), the clear ovalization of the (001) reflection is related to the deformation of the triclinic cell, which in turn depends on its orientation with respect to the draw axis. In isotropic semi-crystalline polymers, one may consider two boundary cases regarding crystal orientation. In crystals with chain axis parallel to the draw direction, the inter-reticular distance between (001) planes tends to increase while the reverse behavior occurs for crystals with chain axis perpendicular to the draw direction. This leads to a shift towards larger Bragg angles in the equatorial region and to a shift towards lower 2θ in the polar zone for the (001) reflection.
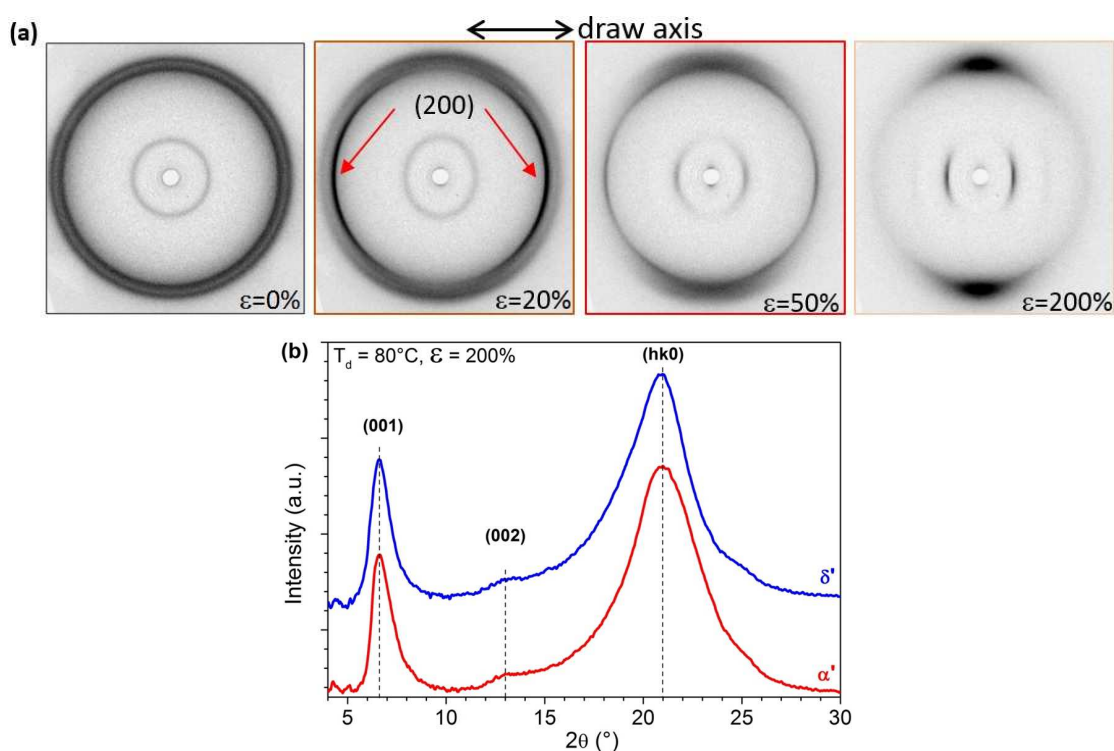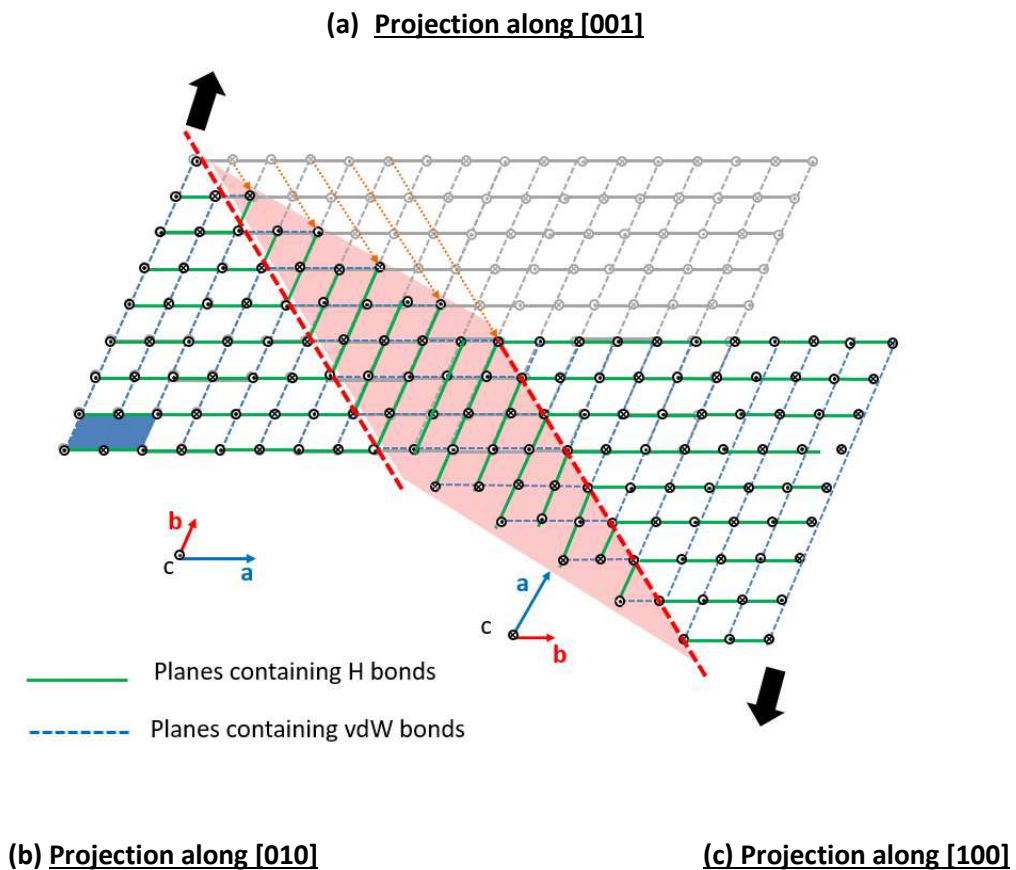
Figure 5. (a) In-situ WAXS patterns of PA11-α' stretched at 80°C as a function of the engineering strain and (b) comparison between stretched PA11 samples initially crystallized under α' and δ' forms.

Moreover, contrary to the (010/210) reflection which is oriented perpendicular to the draw axis from the early stages of deformation, there is a strong intensification of the (200) reflection in the polar region for ε= 20% (as indicated by the red arrows on the figure 5.a). This result indicates that there are more (200) planes normal to the draw direction in the Bragg condition. This phenomenon has already been reported in PA11 and is ascribed to a twinning mechanism which produces a significant reorientation of the lattice with respect to the draw axis [59]. The twinning system is defined by the (200) plane and the twinning direction is a combination of both $[1\bar{2}1]$ and $[001]$ directions as illustrated in Figure 6. This mechanism leads to a reorientation of the (200) and (010) planes with respect to the draw axis. In particular, the (200) planes undergo a change in orientation from parallel to perpendicular to the draw direction as a consequence of twinning, such that they diffract in the polar region.
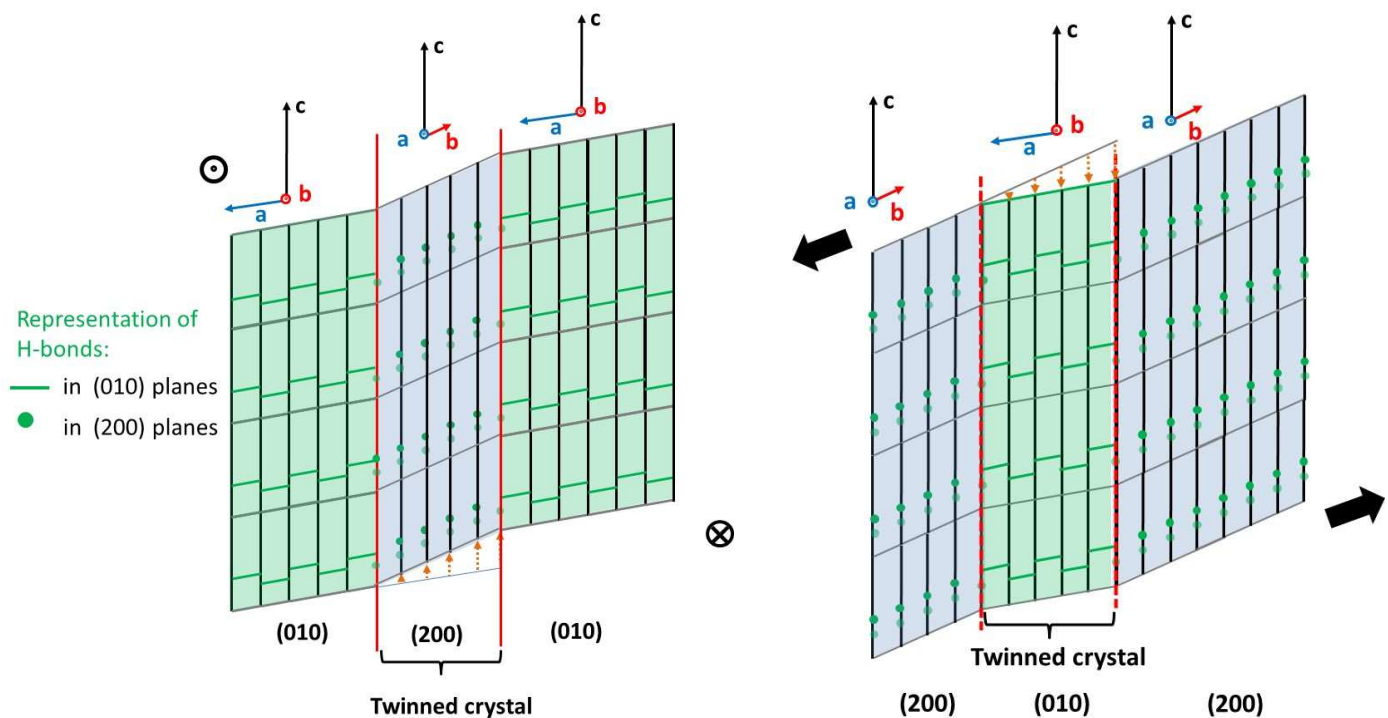
(a) Projection along [001]

Planes containing H bonds

Planes containing vdW bonds

(b) Projection along [010]   **(c) Projection along [100]**

Figure 6. Scheme of twinning mechanism in PA11-α′ sample. Projection along the (a) [100] axis (b) [010] axis (c) [001] axis of the triclinic unit cell.

The SAXS patterns recorded during the uniaxial stretching of a PA11 sample crystallized under α′ phase are depicted in Figure 7.
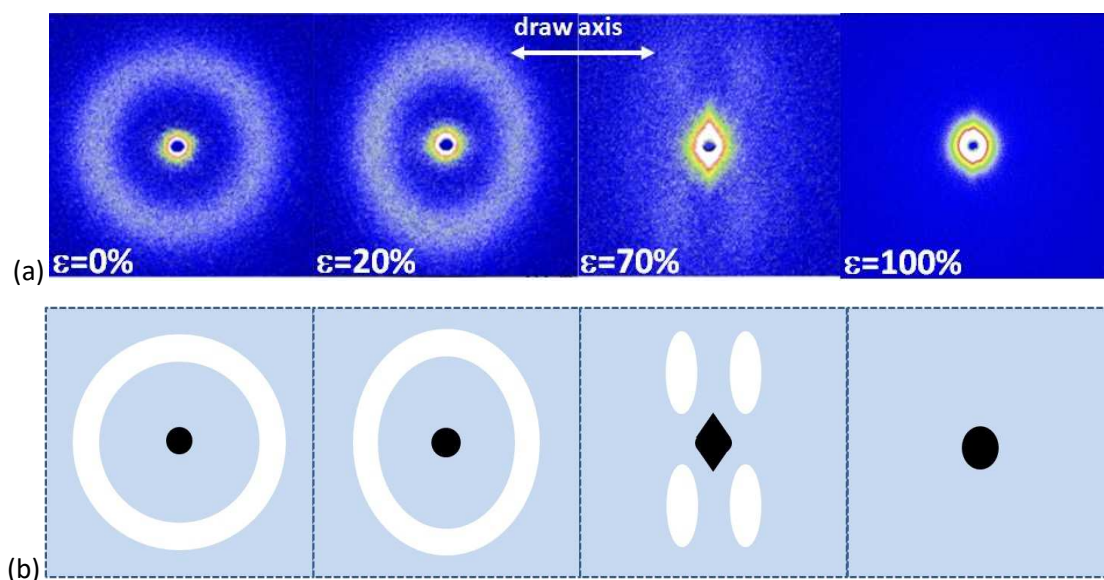

Figure 7. (a) In-situ SAXS patterns and (b) scheme of SAXS patterns of PA11-α′ uniaxially stretched at 80°C.

At low deformations (ε=20%), as observed in the previous case, the initial circular ring transforms into an ellipse reflecting the different states of stress undergone by the lamellae depending on their orientation with respect to the draw direction. When the deformation increases (ε= 70%), the

diffusion ring turns into a four-points pattern located at ±60° from the draw axis, indicating that crystalline lamellae are tilted. Considering that chains orient towards the draw axis as shown previously by WAXS, this suggests that deformation proceeds by a shear mechanism. Moreover, a strong central scattering normal to the draw axis is indicative of the occurrence of a lamellar to fibrillar transformation. In summary, SAXS and WAXS data highlight that the PA11-α'→PA11-δ' transition mainly occurs during the fibrillar transformation. Beyond ε=70%, the very weak scattering reflects the decrease in sample thickness and/or the loss of the regular crystal/amorphous stacks upon drawing as evoked previously. Note that this phenomenon may as well originate from the decrease in electronic contrast between the amorphous and crystalline phases as the order-disorder transformation takes place.

Similar results are obtained for PA6-α uniaxially drawn at 80°C: at low strain, a twinning mechanism is occurred. Then, as the strain is increased, WAXS and SAXS data reveal a fibrillar transformation with a PA6-α→PA6-β transition. However, this transformation is less pronounced than in case of PA11-α' (see supporting information). This result may be related to the higher degree of perfection of the PA6-α.

Strain-induced phase transitions above the Brill transition

The key contribution of in-situ structural characterization is clearly provided by experiments conducted above the Brill transition in order to assess the respective roles of temperature and deformation.

The strain-induced structural change in PA11-δ is studied at 140°C. Characteristic WAXS patterns recorded at different deformation ratios are depicted in Figure 8(a) while the 360° integrated intensity profiles calculated from the WAXS patterns are shown in Figure 8(b). Apart from the gradual orientation of the macromolecular chains along the draw axis, WAXS patterns do not reveal any significant structural changes upon stretching.
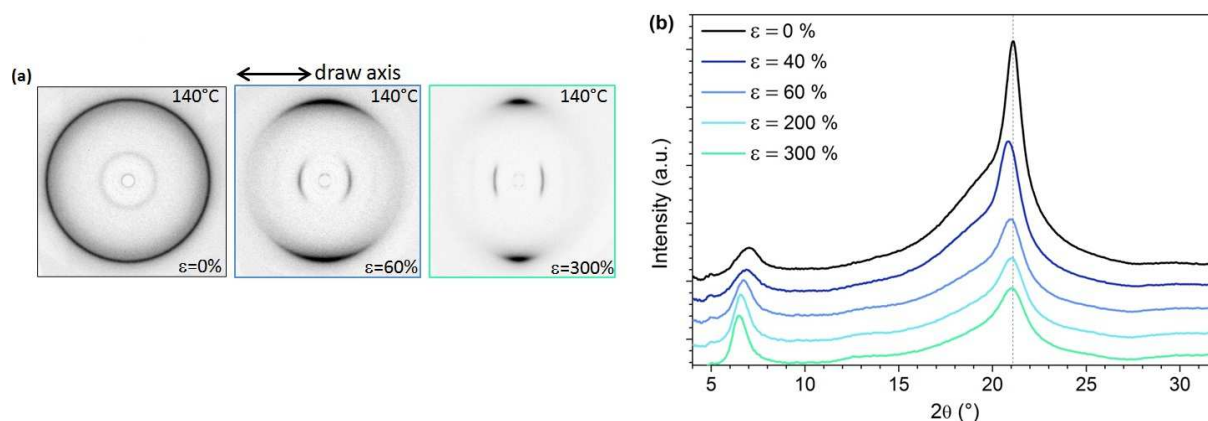
Figure 8. (a) In-situ WAXS patterns of PA11-δ stretched at 140°C as a function of the engineering strain, (b) evolution of diffractograms.

Comparison of the diffractograms before and after uniaxial stretching reveals similar structural organization. As in the case of PA11-δ', only a broadening of the main diffraction and a roughly 10% increase in crystallinity are found. These results suggest that the high temperature δ structure is mechanically stable. In order to confirm that sample was still under the HT structure, the stretched PA11-δ specimen was cooled down to room temperature. The diffractograms of Figure 9 reveal the emergence of the H-bonded sheet-like structure arising from the thermally-induced δ→α' phase transition upon cooling of the stretched sample.
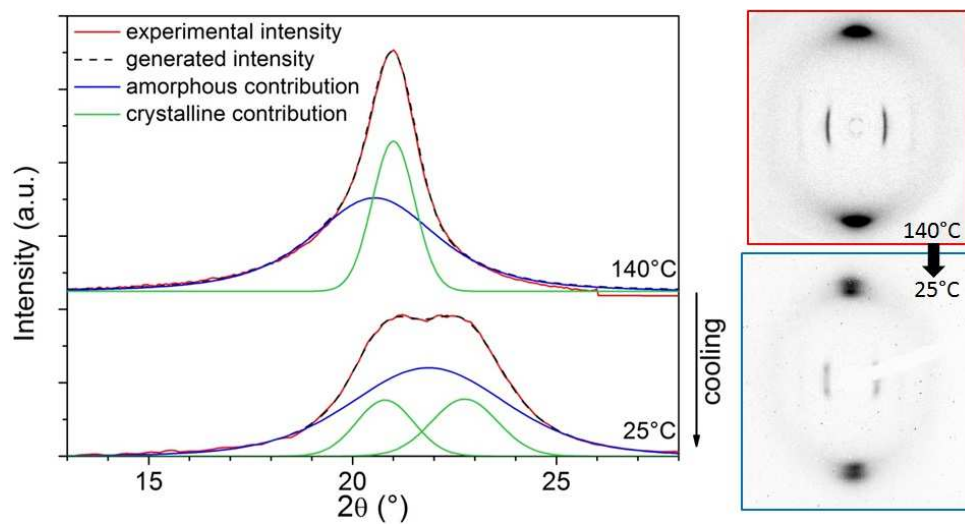

Figure 9. Comparison between PA11-δ stretched at 140°C and after cooling down to room temperature: deconvolution of diffractograms in equatorial plane- ε = 400%

The SAXS patterns recorded at 140°C during stretching are reported in Figure 10. Deformation of the HT form proceeds by a progressive orientation of the lamellae perpendicular to the draw axis as indicated by the polar scattering on the SAXS patterns. Note that contrary to PA11 samples stretched at low temperature, the meridian scattering is strong even at high draw ratio, despite the decrease in sample thickness. This suggests that both regular stacking and electronic contrast between crystalline and amorphous parts persist at high draw ratio.
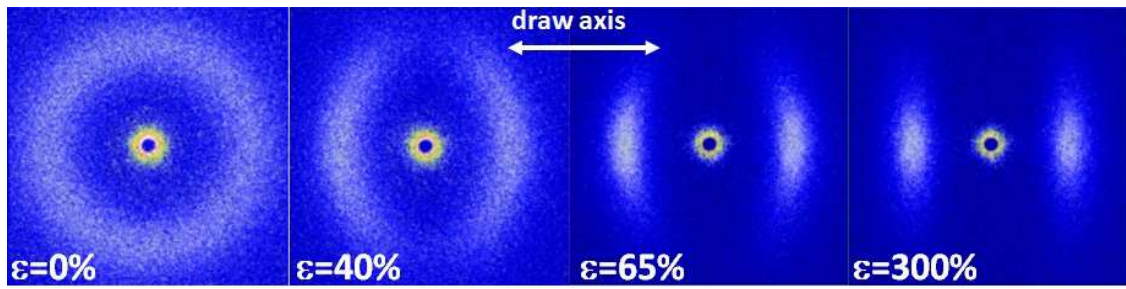
Figure 10. In-situ SAXS patterns of PA11-δ uniaxially stretched at 140°C.

Figure 11(a) illustrates the case of PA6-β' stretched at 140°C. Apart from chain orientation along the draw axis and a broadening of the main reflection attributed to crystal fragmentation, stretching does not seem to induce major crystalline changes. This result appears in apparent contradiction with those reported in previous studies based on post mortem analysis that concluded for a mechanically-induced β into α transformation [5]. In order to identify the nature of the crystalline phase in PA6-β' sample stretched at 140°C, the latter was cooled down to room temperature. Figure 11(b) reveals the emergence of the two well defined diffraction peaks characteristic of the H-bonded sheet like structure. One way to explain this result is to consider that PA6-β' is mechanically stable at 140°C and thermally transforms into the sheet-like structure upon cooling down to RT.
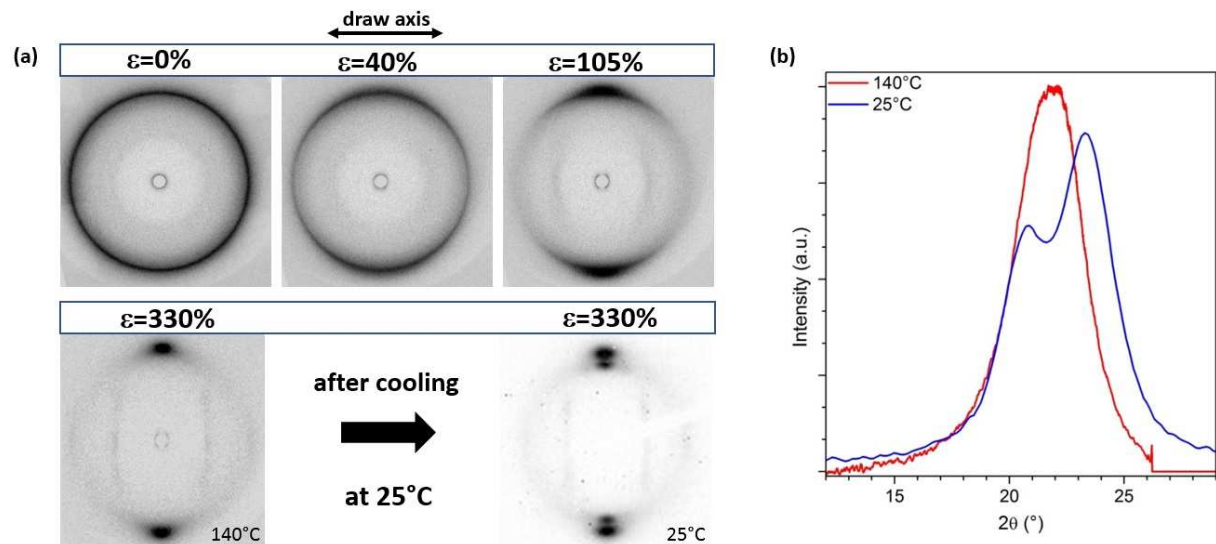

Figure 11. (a) In-situ WAXS patterns of a PA6 sample in β' form stretched at 140°C and (b) equatorial integration before and after cooling down to room temperature.

Structural evolution of PA11-α and PA6-α at high temperature

Figure 12 depicts the structural evolution of PA11-α stretched at 140°C. Similar deformation mechanisms as those activated for PA11-α′ stretched at 80°C (i.e. twinning and fibrillar transformation) are involved, leading to a gradual disappearance of the two main reflections to the benefit of a single diffraction peak centered around 2θ≈21°, characteristic of a (pseudo)hexagonal lattice. Comparison of the equatorial diffractograms of PA11-δ and PA11-α drawn at 140°C shows that both stretched specimens are in the same HT PA11-δ phase. This result is confirmed by the formation of the imperfect sheet-like structure in the stretched PA11-α upon cooling down to room temperature.
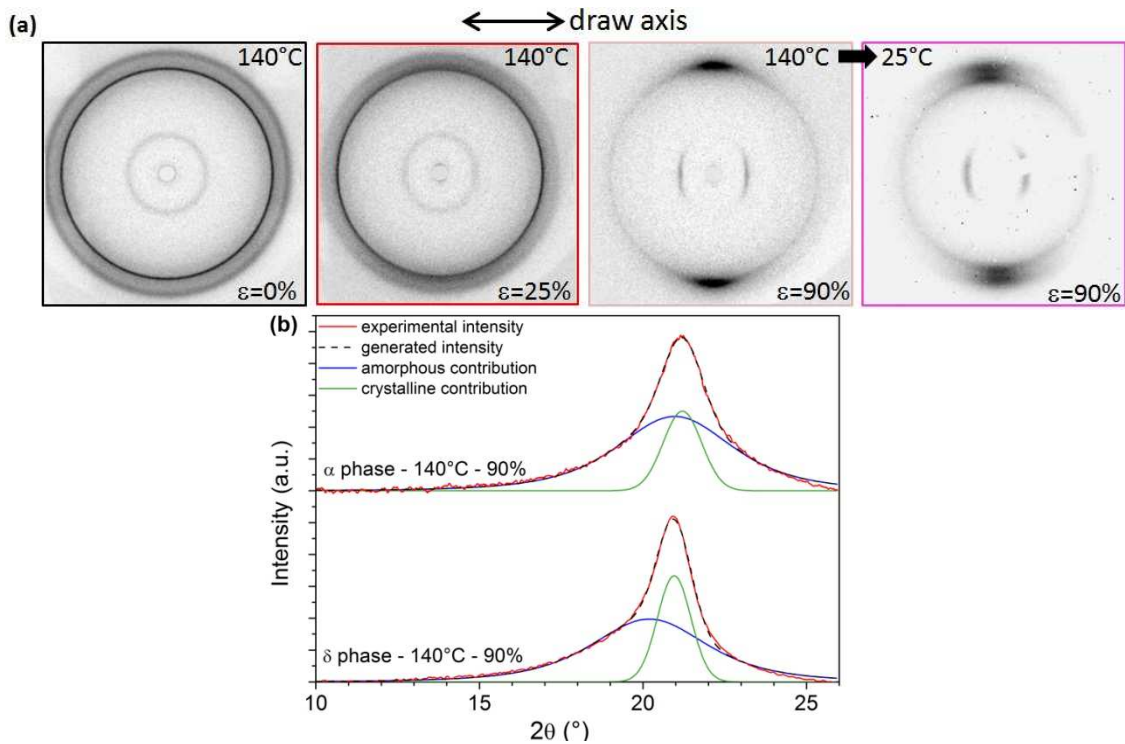

Figure 12. (a) Diffraction patterns of PA11-α stretched at 140°C and (b) comparison of diffractograms in equatorial plane of PA11-δ and PA11-α stretched up to 90 % at 140°C.

Figure 13 displays the evolution of SAXS patterns of PA11-α stretched at 140°C. In addition to the ovalization already observed (ε=25%), an increase in the central scattering without preferential orientation is observed in the early stages of deformation suggesting the formation of spherical cavities. Subsequently, lamellar shearing is observed (ε=40%) and then, for significant deformation ratio, lamellae orient perpendicular to the draw axis. As in the case of PA11-α′ stretched at 80°C, the central diffusion accounts for the fibrillar transformation concomitant to the loss of the characteristic reflections of the α phase in WAXS patterns. Note also that unlike the experiments performed at 80°C, the scattering characteristic of a long period remains visible, even for the highest draw ratios.
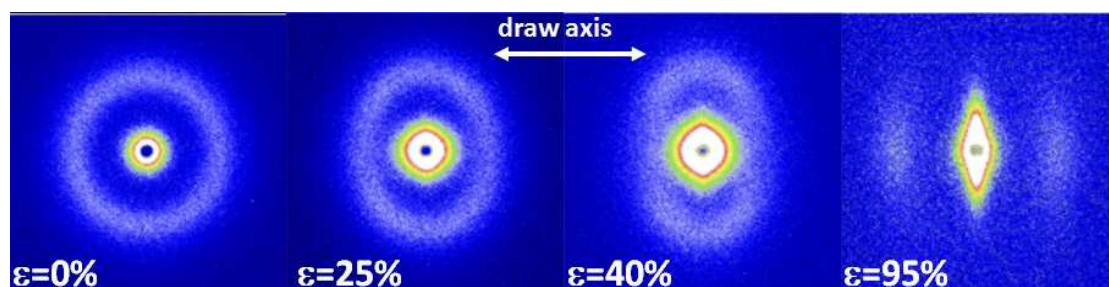
Figure 13. SAXS patterns of PA11-α uniaxially stretched at 140°C.

Figure 14 depicts the structural evolution of PA6 crystallized under α form which is thermally stable at 140°C. As for PA11, the H-bonded sheet like structure is unstable upon uniaxial drawing and transforms into the HT phase. A twinning mechanism also occurs in the early stages of deformation and the two reflections characteristic of the α phase disappear to the benefit of a single reflection attributed to the HT structure. Comparison of the WAXS patterns for both PA6-β' and PA6-α stretched up to 300% at 140°C reveals that the mechanically-induced structure is the same for both samples, i.e. in β' form.

Contrary to what was originally concluded from ex-situ analyses on PA6 [5], all these results highlight the fact that only the H-bonded sheet-like structures in both PA6 and PA11 could be mechanically unstable. They transform into a pseudohexagonal phase in which the H-bonds are randomly distributed around the chain axis. These crystalline transitions occur during the fibrillar structure build-up. This mechanically-induced transformation may explain the ductility of the H-bonded sheet-like structures observed in uniaxial drawing. One may consider that this crystal organization allows activation of more slip systems, thus promoting plasticity. A twinning mechanism is systematically involved prior to this crystallographic change, enabling crystal reorientation so that the H-bonded planes initially normal to the draw direction move towards the draw axis. The brittleness of the H-bonded sheet-like structures as observed under biaxial drawing may indicate that this twinning mechanism is not operative under this state of stress. However further investigations are still necessary to elucidate this point.
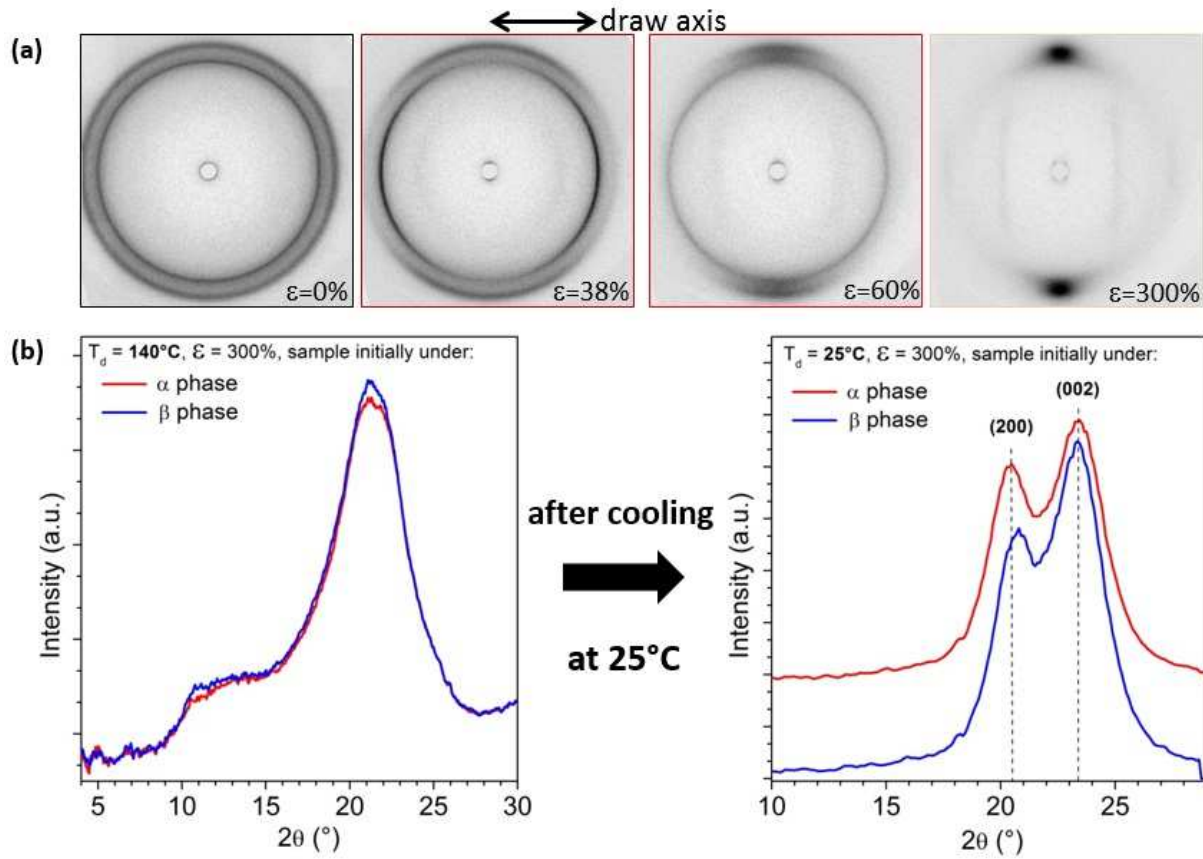
Figure 14. (a) WAXS patterns of PA6-α stretched at 140°C as a function of the engineering strain (b) Comparison of the diffractograms of PA6 samples initially crystallized under α and β forms stretched at 140°C up to 300% at 140°C and after cooling down to room temperature.

Conclusions

The mechanically-induced phase transitions occurring in PA11 and PA6 under uniaxial drawing have been investigated in-situ in relation to the initial crystalline structure. These results provide a general scheme of crystal phase evolution. An order-disorder transition upon uniaxial stretching of the H-bonded sheet like crystal polymorphs into a pseudohexagonal structure in which the H-bonds are randomly distributed around the chain axis. This phase transition may explain the good drawability of the H-bonded sheet-like forms in uniaxial tension. It is established that a twinning mechanism is involved at low deformation, prior to the mechanically-induced crystal phase transitions.

These in-situ investigations provide no evidence of a mechanically-induced phase transition in the case of the mesophases and HT forms, thus assessing that these structures are stable upon uniaxial stretching. It also reveals that in the case of the HT structures the thermally-induced crystal transition known as the Brill transition occurs upon cooling the sample down to room temperature, leading to an oriented H-bonded sheet-like structure.

Author information

Corresponding author

e-mail: valerie.gaucher@univ-lille.fr

Phone: +33 3 20 33 64 16

References

[1]:   V. Miri, O. Persyn, J.M. Lefebvre, R. Séguéla, Effect of water absorption on the plastic deformation behavior of nylon 6, Eur. Polym. J. 45 (2009) 757-762. https://doi.org/10.1016/j.eurpolymj.2008.12.008.

[2]:   E. Parodi, G.W.M. Peters, L.E. Govaert, Prediction of plasticity-controlled failure in polyamide 6: Influence of temperature and relative humidity, J. Appl. Polym. Sci. 135 (2017) 45942. https://doi.org/10.1002/app.45942.

[3]:   M. I. Kohan, Nylon Plastics Handbook, Carl Hanser Verlag: Munich,1995.

[4]:   S. Onogi, T. Asada, Y. Fukui, I. Tashinaka, The mechanical and rheo-optical properties of Nylon 11 and 12, Bulletin of the Institute for chemical research Kyoto university 52 (1974) 368-392. http://hdl.handle.net/2433/76558

[5]:   L. Penel-5 R. Séguéla, J.M. Lefebvre, V. Miri, C. Depecker, M. Jutigny, J. Pabiot, Structural and Mechanical Behavior of Nylon-6 Films. II. Uniaxial and Biaxial Drawing, Polymer 39 (2001) 1224-1236. https://doi.org/10.1002/polb.1096.

[6]:   S. Aharoni, n-Nylons: their synthesis, structure and properties; John Wiley & Sons: New York, 1997, pp. 284-296.

[7]:   N.S. Murthy, Hydrogen bonding, mobility and structural transitions in aliphatic polyamides, J. Polym. Sci., Part B: Polym. Phys. 44 (2006) 1763-1782. https://doi.org/10.1002/polb.20833.

[8]:   A. M. Rhoades, N. Wonderling C. Schick,R. Androsch, Supercooling-Controlled Heterogeneous and Homogenous Crystal Nucleation of Polyamide 11 and Its Effect onto the Crystal/Mesophase Polymorphism, Polymer 106 (2016), ,29–34. https://doi.org/10.1016/j.polymer.2016.10.050

[9]:   Y. Furushima, M. Nakada, K. Ishikiriyama, A. Toda, R. Androsch, E. Zhuravlev, C. Schick, Two crystal populations with different melting/reorganization kinetics of isothermally crystallized polyamide 6, J. Polym. Sci. Polym. Phys. 54 (2016) 2126-2138. https://doi.org/10.1002/polb.24123

[10]:   K.G. Kim, B.A. Newman, J.I. Scheinbeim, Temperature dependence of the crystal structures of Nylon 11, J. Polym. Sci., Part B: Polym. Phys. 23 (1985) 2477-2482. https://doi.org/10.1002/pol.1985.180231206.

[11]:   W.G. Perkins, R.S. Porter, Solid-state deformation of polyethylene and nylon and its effects on their structure and morphology, J. Mater. Sci. 12 (1977) 2355-2388. https://doi.org/10.1007/BF00553923.

[12]:   W.P. Slichter, Crystal structures in polyamides made from ω-amino acids. J. Polym. Sci. 36 (1959) 259-266. https://doi.org/10.1002/pol.1959.1203613020.

[13]:   B.A. Newman, T.P. Sham, K.D. Pae, A high-pressure x-ray study of Nylon 11. J. Appl. Phys 48 (1977) 4092-4098. https://doi.org/10.1063/1.323435.

[14]:   S. Gogolewski, Effect of annealing on thermal properties and crystalline structure of polyamides. Nylon 11 (polyundecaneamide), Colloid Polym. Sci. (1979), 257, 811-819. https://doi.org/10.1007/BF01383352.

[15]:   B. Wunderlich, Macromolecular Physics, vol 1, crystal structure, morphology, defects, Academic Press, 1973.

[16]: H. Arimoto, M. Ishibashi, M. Hirai, Y. Chatani, Crystal structure of the γ form of nylon 6, J. Polym. Sci., Part A: Polym. Chem. 3 (1965) 317-326. https://doi.org/10.1002/pol.1965.100030132.

[17]: T. Sasaki, Notes on the polymorphism in nylon 11, Polym. Lett. 3 (1965) 557-560. https://doi.org/10.1002/pol.1965.110030707.

[18]: A. Kawaguchi, T. Ikawa, Y. Fujiwara, M. Tabuchi, K. Monobe, Polymorphism in lamellar single crystals of Nylon 11, J. Macromol. Sci.-Phys, 20 (1981), 1-20. https://doi.org/10.1080/00222348108219425.

[19]: J.P. Autran, Structure, deformation behavior and properties in polyundecanamide (nylon 11) and high density polyethylene (HDPE) subjected to planar (equibiaxial) deformation by forging. PhD Thesis, University of Massachusetts, 1990.

[20]: E. Balizer, J. Fedderly, D. Haught, B. Dickens, A.S. Dereggi, FTIR and X-ray study of polymorphs of nylon 11 and relation to ferroelectricity, J. Polym. Sci., Part B: Polym. Phys. 32 (1994) 365-369. https://doi-org.inc.bib.cnrs.fr/10.1002/polb.1994.090320219.

[21]: D. Holmes, C. Bunn, D. Smith, The crystal structure of polycaproamide: nylon 6, J. Polym. Sci., Part A: Polym. Chem. 17 (1955) 159-177. https://doi.org/10.1002/pol.1955.120178401.

[22]: N.S. Murthy, Metastable crystalline phases in Nylon 6, Polym. Commun. 32 (1991) 301-305.

[23]: A. Ziabicki, Über die mesomorphe beta-form von polycapronamid und ihre Umwandlung in die kristalline form alpha, Colloid-zeitschrift 167 (1959) 132-141. https://doi.org/10.1007/BF01809631.

[24]: L.G. Roldan, H.S. Kaufman, Crystallization of nylon 6, Polymer letters 1 (1963) 603-608. https://doi.org/10.1002/pol.1963.110011107.

[25]: F. Auriemma, V. Petraccone, L. Parravicini, P. Corradini, Mesomorphic form (ℤ) of nylon 6, Macromolecules 30 (1997) 7554-7559. https://doi.org/10.1021/ma970828e.

[26]: D. Cavallo, L. Gardella, G.C. Alfonso, G. Portale, L. Balzano, R. Androsch, Effect of cooling rate on the crystal/mesophase polymorphism of polyamide 6, Colloid and Polym. Sci. 289 (2011) 1073-1079. https://doi.org/10.1007/s00396-011-2428-6.

[27]: D. Mileva, R. Androsch, E. Zhuravlev, C. Schick, Morphology of mesophase and crystals of polyamide 6 prepared in a fast scanning chip calorimeter, Polymer 53 (2012) 3994-4001. https://doi.org/10.1016/j.polymer.2012.06.045.

[28]: M. Dosiere, JJ. Point, Orientation of the boundary faces innylon-11 lamellar crystals, J Polym Sci: Polym Phys Ed 22 (1984) 1383-98. https://doi.org/10.1016/0032-3861(93)90384-M

[29]: R. Brill, Über das verhalten von polyamiden beim erhitzen, J. Für Praktische Chemie 161 (1942) 49-64. https://doi.org/10.1002/prac.19421610104.

[30]: C. Olmo, R. Rota, J. C. Martınez, J. Puiggal, L. Temperature-Induced Structural Changes in Even-Odd Nylons with Long Polymethylene Segments, J. Polym. Sci. Part B : Polym. Phys. 54 (2016) 2494-2506. https://doi.org/10.1002/polb.24245

[31]: D. Bertoldo Menezes, A. Reyer, M. Musso, Investigation of the Brill transition in nylon 6,6 by Raman, THz-Raman, and two-dimensional correlation spectroscopy, Spectrochimica Acta - Part A: Molecular and Biomolecular Spectroscopy, 190 (2018) 433-441.

https://doi.org/10.1016/j.saa.2017.09.055

[32]:   S.S. Nair, C. Ramesh, K. Tashiro, Crystalline phases in Nylon-11: Studies using HTWAXS and HTFTIR. Macromolecules 39 (2006) 2841-2848. https://doi.org/10.1021/ma052597e.

[33]:   H.J. Radusch, M. Stolp, R. Androsch, Structure and temperature-induced structural changes of various polyamides. Polymer 35 (1994) 3568-3571.
https://doi.org/10.1016/0032-3861(94)90926-1.

[34]:   N.S. Murthy, S.A. Curran, S.M. Aharoni, H. Minor, Premelting crystalline relaxations and phase transitions in Nylon 6 and 6,6. Macromolecules 24 (1991) 3215-3220. https://doi.org/10.1021/ma00011a027.

[35]:   N. Vasanthan, N.S. Murthy, R.G. Bray, Investigation of Brill transition in nylon 6 and nylon 6,6 by infrared spectroscopy. Macromolecules 31 (1998) 8433-8435.https://doi.org/10.1021/ma980935o.

[36]:   J. Pepin, V. Miri, J.M. Lefebvre, New insight into the Brill transition in Polyamide 11 and polyamide 6. Macromolecules, 49 (2016) 564-573. https://doi.org/10.1021/acs.macromol.5b01701.

[37]:   J. Pepin, V. Gaucher, J.M. Lefebvre, A. Stroeks, Biaxial stretching behavior as a probe of H-bond organization in semi-crystalline polyamides, Polymer 101 (2016) 217-224. https://doi.org/10.1016/j.polymer.2016.08.078.

[38]:   Z. Cai, X. Liu, Q. Zhou, Y. Wang, C. Zhu, X. Xiao,D. Fang, H. Bao, The structure evolution of polyamide 1212 after stretched at different temperatures and its correlation with mechanical properties, Polymer 117 (2017) 249-258. https://doi.org/10.1016/j.polymer.2017.04.037

[39]:   L. Wang, X. Dong, M. Huang, D. Wang, Transient microstructure in long alkane segment polyamide: Deformation mechanism and its temperature dependence. Polymer 97 (2016) 217-225. https://doi.org/10.1016/j.polymer.2016.05.038.

[40]   Q. Zhang, Z. Mo, H. Zhang, S. Liu, S.Z.D. Cheng, Crystal transitions of Nylon 11 under drawing and annealing. Polymer, 42 (2001) 5543–5547. https://doi.org/10.1016/S0032-3861(01)00050-7.

[41]   N. Dencheva, Z. Denchev, M. Jovita Oliveira, S.S. Funari, Relationship between crystalline structure and mechanical behavior in isotropic and oriented Polyamide 6, J. Appl. Pol. Sci. 103 (2007) 2242-2252. https://doi-org.inc.bib.cnrs.fr/10.1002/app.25250.

[42]   H. Guo, J. Wang, C. Zhou, W. Zhang, Z. Wang, B. Xu, J. Li, Y. Shang, J. Christiansen, D. Yu, Z. Wu, S. Jiang, Direct investigations of deformation and yield induced structure transitions in polyamide 6 below glass transition temperature with WAXS and SAXS, Polymer 70 (2015) 109-117. https://doi.org/10.1016/j.polymer.2015.06.013.

[43]   L. Penel-Pierron, C. Depecker, R. Séguéla, J.M. Lefebvre, Structural and mechanical behavior of Nylon 6 films Part I. Identification and stability of the crystalline phases, J. Polym. Sci., Part B : Polym. Phys. 39 (2001) 484-495.
https://doi.org/10.1002/1099-0488(20010301)39:5<484::AID-POLB1022>3.0.CO;2-R.

[44]   V. Miri, O. Persyn, J.M. Lefebvre, R. Séguéla, A. Stroeks, Strain-induced disorder–order crystalline phase transition in nylon 6 and its miscible blends, Polymer 48 (2007) 5080-5087. https://doi.org/10.1016/j.polymer.2007.06.039.

[45]   N.S. Murthy, R. Bray, S. Correale, R. Moore, Drawing and annealing of nylon-6 fibres: studies of crystal growth, orientation of amorphous and crystalline domains and their influence on properties. Polymer 36 (1995) 3863–3873. https://doi.org/10.1016/0032-3861(95)99780-X.

[46]   J.R. Xu, X.K. Ren, T. Yang, X.Q. Jiang, W.Y. Chang, S. Yang, A. Stroeks, E.Q. Chen, Revisiting the thermal transition of β-form Polyamide-6: evolution of structure and morphology in uniaxially stretched films, Macromolecules 51 (2018) 137-150. https://doi.org/10.1021/acs.macromol.7b01827.

[47]:   D.L. Wang, C.G. Shao, B.J. Zhao, L.G. Bai, X. Wang, T.Z. Yan, J.J. Li, G.Q. Pan, L.B. Li, Deformation-induced phase transitions of polyamide 12 at different temperatures: an in situ wide-angle X-ray scattering study, Macromolecules 43 (2010) 2406-2412. https://doi.org/10.1021/ma1000282.

[48]:   Z. Cai, H. Bao, C. Zhu, S. Zhu, F. Huang, J. Shi, Structure evolution of polyamide 1212 during the uniaxial stretching process: in situ synchrotron wide-angle X Ray diffraction and small-angle X-Ray scattering analysis, Ind. Eng. Chem. Res.55 (2016) 7621-7627. https://doi.org/10.1021/acs.iecr.6b00643

[49]   C. Millot, R. Séguéla, O. Lame, L.A. Fillot, C. Rochas, P. Sotta, Tensile deformation of bulk Polyamide 6 in the preyield strain range. Micro–macro strain relationships via in situ SAXS and WAXS, Macromolecules 50 (2017) 1541-1553. https://doi.org/10.1021/acs.macromol.6b02471.

[50]   M. Inoue, Studies on crystallization of high polymers by differential thermal analysis, J. Polym. Sci. Part A: Polym. Chem. 1 (1963) 2697-2709. https://doi.org/10.1002/pol.1963.100010813.

[51]   B. Wunderlich, Macromolecular Physics; academic Press: New York, 1980, vol 3, crystal melting

[52]   N.S. Murthy, M.K. Akkapeddi, W.J. Orts, Analysis of lamellar structure in semi-crystalline polymers by studying the absorption of water and ethylene glygol in nylons using small-angle neutron scattering, Macromolecules 31 (1998) 142-152. https://doi.org/10.1021/ma9707603.

[53]   R. Séguéla, On the strain-induced crystalline phase changes in semi-crystalline polymers: Mechanisms and incidence on the mechanical properties, J. Macromol. Sci.- Pol. R. 45 (2005) 263-287. https://doi.org/10.1081/MC-200067727.

[54]   L. Wang, X. Dong, M. Huang, D. Wang, Transient microstructure in long alkane segment polyamide: Deformation mechanism and its temperature dependence, Polymer 97 (2016) 217-225. https://doi.org/10.1016/j.polymer.2016.05.038

[55]   L. Wang, X. Dong, M. Huang, A. J. Muller, D. Wang, The effect of microstructural evolution during deformation on the post-yielding behavior of self-associated polyamide blends, Polymer 117 (2017) 231-242. https://doi.org/10.1016/j.polymer.2017.04.038

[56]   S. Humbert, O. Lame, J.M. Chenal, C. Rochas, Small strain behavior of Polyethylene: in situ SAXS measurements, J. Polym. Sci., Part B: Polym. Phys. 48 (2010) 1535–1542. https://doi.org/10.1002/polb.22024.

[57]   K. Djezzar, L. Penel, J.M. Lefebvre, R. Séguéla, Y. Germain, Tensile drawing of ethylene/vinyl-alcohol copolymers. Part 1. Influence of draw temperature on the mechanical behaviour, Polymer 39 (1998) 3945–3953. https://doi.org/10.1016/S0032-3861(97)10349-4.

[58]   V. Miri, O. Persyn, R. Séguéla, J.M. Lefebvre, On the deformation induced order–disorder transitions in the crystalline phase of polyamide 6, Eur. Polym. J. 47 (2011) 88–97. https://doi.org/10.1016/j.eurpolymj.2010.09.006.

[59]   L. Jolly, A. Tidu, J.J. Heizmann, B. Bolle, Microstructure evolution in polyamide PA11 under small uniaxial extension, Polymer 43 (2002) 6839-6851. https://doi.org/10.1016/S0032-3861(02)00486-X.